An overview of optical coherence tomography for ovarian tissue imaging and characterization

Tianheng Wang,
Department of Electrical and Computer Engineering, University of Connecticut, Storrs, CT 06269, USA

Molly Brewer, and
Division of Gynecologic Oncology, University of Connecticut Health Center, Farmington, CT 06030, USA

Quing Zhu[*]
Department of Electrical and Computer Engineering & Department of Biomedical Engineering, University of Connecticut, Storrs, CT 06269, USA

Abstract

Ovarian cancer has the lowest survival rate among all the gynecologic cancers because it is predominantly diagnosed at late stages due to the lack of reliable symptoms and efficacious screening techniques. Optical coherence tomography (OCT) is an emerging technique that provides high-resolution images of biological tissue in real time, and demonstrates great potential for imaging of ovarian tissue. In this paper, we review OCT studies for visualization and diagnosis of human ovaries as well as quantitative extraction of ovarian tissue optical properties for classifying normal and malignant ovaries. OCT combined with other imaging modalities to further improve ovarian tissue diagnosis is also reviewed.

Introduction

Optical coherence tomography (OCT) is an emerging high resolution and noninvasive imaging technique that can perform cellular level imaging.[1–4] It measures backscattered light from microstructural features within the examined tissues. OCT typically achieves a resolution of several microns and a penetration depth of a few millimeters. OCT technique and systems have advanced rapidly since it was first demonstrated in 1991,[5] from free-space to fiber-based configurations, from time-domain to Fourier-domain systems, from intensity-based OCT to different types of functional OCT, including polarization-sensitive OCT (PS-OCT),[6,7] Doppler OCT [8–11] and spectroscopic OCT.[12–14] OCT has been used to image biological tissues in human body and demonstrated great potential for clinical applications,[15–17] including the ophthalmology,[18–20] dentistry,[21–23] gastrointestinal (GI) tract,[24,25] coronary blood vessels,[26–28] colon,[29] breast,[30–32] and so forth.

[*]zhu@engr.uconn.edu.

Ovarian cancer ranks fifth in cancer deaths, and has the highest mortality rate among all the gynecologic cancers with a 5-year survival rate of 44% or less. There are approximately 21,980 estimated new cases of ovarian cancer in the United States in 2014 and an estimated 14,270 deaths.[33] The majority of ovarian cancer cases are diagnosed at Stage III or IV due to ambiguous early symptoms as well as poor screening techniques. The serum tumor marker CA 125 yields a sensitivity of less than 50%; transvaginal ultrasound has only 3.1% positive predictive value; pelvic exams yield a low sensitivity of only 30% or less; computed tomography (CT) scan for ovarian cancer detection achieves a specificity of 85%, but the sensitivity is only 45%.[34–38] However, given the lack of better technologies, CA125, ultrasound and other serum markers are currently being use for screening in high risk women. There is no effective diagnostic tool for early detection of ovarian cancer for high-risk women who carry a BRCA mutation or another genetic alteration that substantially increases the risk of ovarian cancer. Two landmark studies on prophylactic oophorectomy (PO) for women who carry BRCA 1 or BRCA 2 mutations were reported in 2002.[39,40] PO reduces the risk of ovarian cancer, and has been accepted as the standard of care for high-risk women. However, there appears to be a higher mortality rate associated with premenopausal oophorectomy. These high-risk women are not candidates for hormone replacement therapy due to their increased risk of breast cancer.[41] It has been found that PO increases the mortality of women undergoing oophorectomy before the age of 45 [41] or even before the age of 55 to 60.[42] Therefore, there is an urgent need to develop effective tools to detect and diagnose ovarian cancer, so that unnecessary surgery can be avoided, the mortality rate can be reduced, and the quality of patients' life can be improved. OCT is sensitive to collagen changes which are related to the development of malignancy in ovarian tissue,[43] and is capable of detecting morphological features of pre-neoplastic or early neoplastic changes of early-stage ovarian cancer. In this paper, we provide an overview of the utility of OCT for ovarian tissue imaging and characterization. First, the basic principle of OCT is briefly introduced. Second, we review intensity-based OCT studies for ovarian tissue imaging and characterization. Following the intensity-based OCT, the application of PS-OCT on ovarian tissue characterization is reviewed. At the end, we discuss the combination of OCT with other imaging modalities to further improve ovarian cancer detection and diagnosis.

Basic principle of optical coherence tomography

OCT is analogous to ultrasound imaging, except that OCT uses light instead of sound. Figure 1 is a typical time-domain OCT system configuration. It consists of a Michelson interferometer with a low coherence light source. The low coherence light is split into reference and sample arm by a beamsplitter. The light incident on the sample is focused by a focal lens. The back-reflected light from the sample and reference mirror is recombined at the beamsplitter. If the difference of optical path length between reference and sample arm is within the coherence length of the light source, the recombined beam can generate interference signals, which can be detected by a photodetector. B-scan images of the sample can be obtained by scanning the light beam laterally. By performing a two-dimensional spatial scanning, 3D images of the sample can be reconstructed. The axial resolution of the OCT system depends on the central wavelength and bandwidth of the light source. The

lateral resolution is determined by the size of the focused beam, which is determined by the wavelength of the light and the numerical aperture of the focal lens. The system described above is a typical time-domain OCT setup. Fourier-domain OCT (FD-OCT), implemented either as spectral-domain OCT or swept-source OCT, has demonstrated a higher sensitivity and a faster data acquisition speed as compared with the time-domain OCT.[44,45] In FD-OCT, the reference mirror is stationary and the depth information is obtained by the inverse Fourier transform of the detected spectrum in k-space.

Intensity-based OCT for ovarian tissue imaging

Intensity OCT images of ovarian tissue

OCT has been used to image microstructural features of ovarian tissue both *ex vivo* and *in vivo*.[43,46–58] The feasibility of high resolution OCT for differentiating normal and abnormal or malignant ovarian tissue has been demonstrated. Example OCT images acquired by intensity-based OCT and the corresponding histology of ovarian tissue with different morphological structures are shown in Figure 2.[43] The imaged ovaries were divided into four categories of normal, high risk, endometriosis, and neoplasms. The normal ovary (Figure 2a) shows small cysts, a small blood vessel. The epithelium is fairly distinct across the whole ovarian surface. One high-risk ovary (Figure 2b) displays the wavy pattern on the subsurface of the ovary. However, it may not be diagnostic since it has been noticed in all four categories of ovaries. Another high-risk ovary (Figure 2c) displays a normal large follicular cyst. Endometriosis (Figure 2d) shows irregular surface profile, consisting of loose tissue on top of the ovary. Hypointense bands corresponding to connective tissue were observed in both OCT image and histology. Malignant ovarian tissue (Figure 2e) shows a strong birefringence band corresponding to a region of high collagen content. A second ovarian cancer case (Figure 2f) displays 'holes' in the OCT image that histologically correspond to areas of necrotic tumor. Some other structural features in ovarian tissue can be detected by OCT as well, such as lymphocyte (Figure 3a, 3b) and tumor nodule (Figure 3c, 3d).[46]

Based on those studies,[43,46–58] OCT is able to visualize microstructural ovarian features, including stroma, epithelium, collagen, blood vessel, follicle, cyst, corpus luteum, corpus albicans, lymphocyte, calcification, papillary structure, and necrotic tumor. OCT images can readily provide information on normal and abnormal or malignant ovarian tissue. In general, the normal ovarian stroma appears homogeneous and relatively hyperintense in OCT images. Carcinomas appear as either circumferential bumps on the surface or hyperintense irregular regions embedded in signal-poor images. Large blood vessels appear as distinct signal-poor bands in OCT images, which are common in malignant ovaries as the cancer invades tissue. The blood vessels can be detected with high contrast by Doppler OCT. Cysts and follicles appear as signal void or signal poor regions of variable sizes with well-defined boundaries. Collagen regions display hypointense birefringence bands. However, the dense collagen fiber bundles display hyperintense regions in OCT image. Endometriosis is identified by superficial loose connective tissue that is characteristic of endometriosis. Corpus albicans, lymphocytes and calcifications appear as signal void or signal poor regions with variable sizes and shapes. The benign calcified, ossified dermoid tumor appears

heterogeneous in OCT images. Overall, OCT shows particular patterns of backscattered intensity that are different between normal and abnormal ovarian tissue.

Quantitative analysis of OCT for ovarian tissue characterization

In addition to differentiating malignant from normal ovarian tissue utilizing morphological structures, quantitative analysis of scattering properties of ovarian tissue using OCT provides additional information for ovarian tissue characterization. Collagen is the main scatter source in the stroma underlying the epithelium, and collagen content and directivity in stroma may change as pre-cancer or cancer develops.[59] OCT is capable of quantitatively estimating total attenuation coefficient (μ_t) by fitting the A-line measurements.[60,61] Total attenuation coefficient μ_t is the summation of the light absorption coefficient (μ_a) and scattering coefficient (μ_s). Absorption and scattering coefficients describe the fractional attenuation in light intensity per unit distance traversed resulting from absorption and scattering, respectively. As μ_a is much smaller than μ_s for the wavelengths used in OCT, μ_s is approximately equal to μ_t and it is a good estimate of the local scattering properties. Therefore, the quantitative μ_s extracted from OCT A-lines could reflect the local collagen content. For weakly scattering media ($\mu_s < 6$ mm^{-1}) like human ovarian tissue, the single scattering model is valid to extract μ_s; for highly scattering media, the multiple scattering needs to be considered. In the single scattering model, the OCT signal is given by Beer's

law $I(z) = I_0 \sqrt{\exp(-2\mu_s z)}$, where z is the distance in light propagation direction. Thus, the light attenuates exponentially as it penetrates deeper in the biological tissue. The OCT signal *I(z)* refers to the amplitude of the interference signal, the factor 2 accounts for the round trip attenuation and the square-root accounts for the fact that OCT measures the light amplitude instead of the intensity.

In order to investigate the difference of the scattering property between normal and malignant ovarian tissue, optical scattering coefficient was quantitatively extracted from OCT intensity image. Figure 4 shows one set of examples from normal (Figure 4a–4c) and malignant (Figure 4d–4f) ovarian tissue.[47] The inset in Figure 4a shows an example of fitting μ_s. μ_s was estimated by fitting the averaged A-lines to the single scattering model. The μ_s extracted from the OCT fitting areas marked as the white dashed region in Figure 4a and 4d are 2.86 mm^{-1} and 1.29 mm^{-1}, respectively. Picrosirius red stain that specifically binds to collagen was used to stain the histology slides. The stained red area in Figure 4c and 4f represents collagen. The collagen amount, structure, and arrangement are quite different between normal and malignant ovarian tissues. The normal ovary exhibits almost exclusively collagen with interspersed stromal cells and the collagen fibril is randomly oriented and wavy interlaced; the collagen fibers in the malignant tissue are unidirectionally organized into thicker bundles. The amount of collagen was quantitatively analysed using ImageJ. Collagen area fraction (CAF) was measured as 'stained collagen area /tissue area.' A larger amount of collagen is found in normal ovarian tissue (CAF = 58.3%) than in malignant tissue (CAF = 8.4%). A quantitative study was performed on a total of 18 ovaries from 10 patients. The average μs obtained from the normal ovarian tissue was 2.41 mm^{-1} (±0.59), while the average μs obtained from the malignant ovarian tissue was 1.55 mm^{-1} (±0.46). The average CAF obtained from the normal group was 48.4% (±12.3%), while the

average CAF obtained from the malignant group was 11.4% (±4.7%). A statistical significance of both the scattering coefficient and collagen content was found between the two groups (p < 0.001). The changes in collagen can be an indicator of malignancy, and quantitative analysis of optical scattering coefficient from OCT images could be a promising method for detection of early ovarian cancer.

Considering the different collagen distributions between normal and malignant ovarian tissue, angle-resolved optical scattering properties measured from different OCT imaging planes were quantitatively extracted.[48] For each ovary sample, 90 OCT B-scan images were obtained by illuminating the light beam at 5 different incident angles (−36, −18, 0, 18, 36 degrees) and 18 different imaging planes ranging from 0 to +170 degrees with the ovarian sample rotated at 10 degree steps. The positions of the OCT probe were pre-calculated and adjusted to assure the same region of the sample was imaged on each imaging plane. The optical scattering coefficient was extracted from each image. For each imaging plane, the 5 scattering coefficients calculated from 5 different illumination angles formed a dataset. Mean cross correlation coefficient (MCC) was introduced to characterize and differentiate normal and malignant ovaries. MCC is the mean value of cross correlation coefficients between 18 different datasets and measures the angle-resolved scattering similarity between different imaging planes. Figure 5 is an example comparing normal and malignant ovaries. The 18 datasets of angle-resolved scattering coefficient measured from 18 different imaging planes were plotted as a function of light illuminating angle using different color curves (Figure 5a, 5b). The angle distribution of the 18 normal datasets is quite similar, however, this similarity does not exist in malignant ovaries. The calculated MCC for normal and malignant imaging areas are 0.87 and 0.22, respectively. The corresponding OCT images and picrosirius red stained histology images are shown in Figure 5c–5f. There are large differences between normal and malignant cases in terms of collagen content, fiber structure and directionality. Similar to Figure 4c and 4f, the normal ovary exhibits almost exclusively collagen with interspersed stromal cells. The collagen fibers are randomly oriented and run in a wavy course. The malignant ovary has less collagen content with collagen fibers unidirectionally organized into thick bundle embedded around nests of malignant cells. The collagen near the ovarian surface forms a more homogenous network in the normal ovary than that in the malignant one. Therefore, normal ovarian tissue has higher cross correlation value among different angled-resolved imaging planes than malignant ovarian tissue. The average MCC values of 6 normal and 4 malignant ovaries are 0.78 (±0.11) and 0.42 (±0.15), respectively. 100% sensitivity and specificity were achieved by setting a MCC threshold at 0.6 in this limited sample pool. The changes and the distribution in collagen content between normal and malignant ovary effectively explains the different scattering properties in normal and malignant ovarian tissue. By integrating light illumination at various angles over different OCT imaging planes in one scanning mechanism, this technique could be utilized for *in vivo* optical biopsy.

Polarization-sensitive OCT for ovarian tissue imaging

PS-OCT as a functional extension of intensity-based OCT, provides enhanced image contrast and additional physiological information by making use of relative phase of two orthogonal polarization states, and is able to study the polarization properties and measure

birefringence of biological tissue.[6,62] PS-OCT has been reported as an effective tool to detect collagen fibrous tissues, including retinal nerve fiber layer tissue,[63–65] carious lesions,[66,67] collagen content in atherosclerotic plaques,[68,69] collagen fibrous tissue in human skin.[70–72] PS-OCT is capable of detecting birefringence changes caused by collagen, and collagen change in human ovary is an indicator of malignancy. Therefore, PS-OCT could be an effective tool to detect ovarian cancer.[73,74]

Phase retardation images of ovarian tissue

In PS-OCT, the sample is illuminated with circularly polarized light. The backscattered light from the sample is combined with the reference light, which provides equal reference power for both orthogonal polarization channels. The combined light is separated by a polarization beamsplitter into horizontal and vertical components which are detected by two identical photodetectors. PS-OCT intensity image is obtained by calculating the summation of the intensity of two orthogonal channels, while phase retardation image is obtained by calculating the arctangent between vertical and horizontal polarization components. Figure 6 shows one example comparing normal (Figure 6a, 6b) and malignant (Figure 6c, 6d) ovarian tissue. Figure 6a and 6c are intensity OCT images, while 6b and 6d are phase retardation images.[73] The dark blue represents phase retardation value of 0 degree and the dark red represents 90 degrees. The phase retardation of the normal ovarian tissue (Figure 6b) increases uniformly and is slightly dependent on the depth. However, the phase retardation of the malignant ovarian tissue (Figure 6d) is more random with red spots scattered in the image sporadically.

Quantitative analysis of PS-OCT for ovarian tissue characterization

In order to quantitatively classify normal and malignant ovaries, a three-parameter prediction model based on analysis of PS-OCT was developed.[73,74] Three parameters were extracted from PS-OCT intensity and phase images. Optical scattering coefficient was estimated by numerically fitting averaged OCT A-lines to a single scattering model as discussed earlier; phase retardation was obtained by calculating the average phase values from PS-OCT phase images of the same area; phase retardation rate was calculated by linearly fitting the slope of the phase retardation over the depth. Among the 33 ovaries (26 normal and 7 malignant) from 18 patients imaged by PS-OCT, normal ovaries show higher average values of scattering coefficient, phase retardation and phase retardation rate than those of malignant ones, with the normal/malignant ratio of 1.36, 1.11 and 1.77, respectively. The differences in scattering coefficient and phase retardation rate between normal and malignant groups are statistically significant. Linear regression analysis (Figure 7a) shows positive correlation between collagen content and optical scattering coefficient with Pearson's correlation coefficient R=0.57. Phase retardation (Figure 7b) and phase retardation rate (Figure 7c) measured from ovaries are also positively correlated with collagen content with R=0.47, and R=0.74. A multiple linear regression shows that those three parameters together positively correlate with collagen content with R=0.76, which is higher than using each parameter alone. Collagen is associated with the development of ovarian cancers; the collagen amount and structure are quite different between normal and malignant ovaries. Since collagen content fraction, measured from picrosirius red staining on ovary samples, directly assesses collagen, the highly positive correlation indicates that

those three parameters may measure the complicated process of collagen changes in ovarian cancer.

A logistic model was used to classify normal and malignant ovaries. Logistic regression is a statistical modelling approach that can be used to describe the relationship of several predictor variables to a dichotomous response variable 0 or 1. The three extracted parameters from PS-OCT were used as input predictors; the response 1 represents malignant ovary and 0 represents normal ovary. The coefficients of the model that best follow the actual diagnosis were estimated first, and the responses were calculated by using those estimated coefficients. Normal and malignant ovaries could be classified by setting a threshold for the calculated responses. The three parameters extracted from 33-ovary images were used to train the logistic classifier, and 10 additional ovaries (6 normal and 4 malignant) from 5 patients were tested using the trained logistic prediction model. The performance of the logistic prediction model was evaluated using receiver operating characteristic (ROC) curve and the area under the curve (AUC). 100% sensitivity and specificity were achieved in the training group, and 100% sensitivity and 83.3% specificity were achieved in the testing group. The initial results demonstrate that the three-parameter prediction model based on PS-OCT could be a valuable tool to evaluate ovarian tissue for malignancy.

Combining OCT with other modalities for ovarian cancer detection

The combination of OCT with other imaging techniques would provide more diagnostic information of ovarian tissue, which has prompted the development of multi-modality imaging systems and probes. The following sections will review the OCT combined with other modalities for ovarian tissue imaging and characterization.

OCT/positron detection

Positron emission tomography (PET) can detect malignant cancers with altered glucose metabolism using ^{18}F-FDG as a tracer. Positron detection probe is selectively sensitive to short-range beta radiation caused by local tissue uptake of ^{18}F-FDG and is highly sensitive to early-stage cancers.[75,76] A hybrid intraoperative device consists of scintillating fibers and an OCT catheter probe [77] has been developed for simultaneously mapping of local ^{18}F-FDG uptake and morphologic changes of ovarian tissue.[46,49] OCT images revealed many detailed morphological features of abnormal and malignant ovaries, which could be valuable for evaluating local regions with high metabolic activities and detecting early malignant development in ovarian tissue. In this pilot study of 10 patients, positron count rates of malignant ovaries were 7.5/8.8-fold higher than that of abnormal/normal ovaries.[46] An example of a normal ovary from a 58-year-old postmenopausal patient is shown in Figure 8a–8c. Figure 8a shows the positron distribution map, 8b provides one representative B-scan OCT image selected from a sequence of co-registered OCT images, and 8c is the corresponding histology. As shown in Figure 8a, photons received from eight scintillating fibers were distributed within the corresponding positions (circles). The total positron count rate was 0.95 counts/MBq. The homogeneous OCT image had some bright spots near the tissue surface that correspond to dense cortical stroma in histology. An example of an advanced ovarian carcinoma from a 61-year old postmenopausal patient is shown in Figure

8d–8f. The total positron count rate (Figure 8d) was 28-fold higher than was measured in normal ovaries. OCT images revealed irregular patterns of hyperintense regions (Figure 8e, marked by arrows) which represent a change in shape and directionality of the collagen fibers. This type of collagen distribution was seen in early cancers but was more dramatic in this example. The histology shows thick collagen bundles embedded in the tumor cells (Figure 8f) which correspond to OCT hyperintense regions (Figure 8e). These results demonstrate the clinical potential of this novel dual-modality device for sensitive detection of ovarian cancer.

OCT/Ultrasound/photoacoustic imaging

Photoacoustic imaging (PAI) has emerged as a promising biomedical imaging modality and demonstrated great potential for medical applications.[78,79] In photoacoustic imaging, a broadband ultrasound transducer is used to measure the acoustic waves generated from thermal expansion of biological tissue caused by the absorption of short laser pulses. The spatial and axial resolution of PAI is determined by the central frequency and bandwidth of the ultrasound transducer. The depth of penetration is scalable with ultrasound frequency, provided that enough light fluence is delivered. In the diagnostic frequency range of 3 to 8 MHz, the penetration depth in tissue can reach 2 to 3 cm using near infrared light. If a higher frequency transducer is used, sub-millimeter resolution can be achieved, however, the depth of penetration is compromised to several millimeters. The light absorption distribution which directly relates to tumor angiogenesis can be obtained from the received photoacoustic signals. Currently, *ex vivo* and *in vivo* studies using a co-registered transvaginal US and PAI imaging probe for non-invasive evaluation of ovaries are under intensive investigation.[80–82] In the study reviewed here, we have investigated the combined OCT, US and PAI utilizing OCT and a high frequency ultrasound transducer of 40 MHz for sub-surface ovarian tissue imaging and characterization. This tri-modality probe would provide complementary information of high-resolution surface morphology and optical scattering (OCT), deeper tissue structures (US), and optical absorption or tissue vascular contrast (PAI). An endoscope probe of 5mm diameter combining the three imaging modalities was developed and tested using *ex vivo* ovaries.[50] Figure 9a shows the design of the endoscopic probe which consists of a ball-lensed OCT fiber, a multimode fiber with the distal end polished at 45 degree for delivering the laser beam for PAI, and a high-frequency ultrasound transducer. The photograph of the probe is shown in Figure 9b. The diameter of the ball-lensed OCT fiber, PAI-light-delivering fiber, and the ultrasound transducer is 0.5mm, 0.9mm and 0.9mm, respectively.

Figure 10a–10d shows one set of images of an abnormal ovary from a 44-year-old premenopausal patient with endometriosis. OCT image (Figure 10a) shows shallow tissue features and a well-defined boundary indicating the presence of a big follicle underneath. The bright spots indicated by pink arrows represent collagen bundles that also show up in the histology (Figure 10d). The US image (Figure 10b) shows a big follicle with clearly identified shape and bottom structures too deep for OCT to adequately image them. PAI (Figure 10c) reveals a very high optical absorption at the surface, which corresponds to a significant amount of red blood cells confirmed with histology resulting from endometriosis. Figure 10e–10h shows images obtained from a malignant ovary of a 61-year-old

postmenopausal patient. The OCT image (Figure 10e) shows many small vessels in the shallow subsurface of approximately 1mm deep that were confirmed by histology shown in Figure 10h indicated by the red arrows. The US image (Figure 10f) shows homogeneous structures near the tissue surface and heterogeneous texture patterns below 1mm. The PAI (Figure 10g) shows many small vessels near the surface of approximately 1mm deep, which agrees with the findings from both the OCT and histology images. The pathology result reveals a high-grade adenocarcinoma with abundant tumor cells below the surface as marked by the yellow diamond arrow, about 1mm below the surface. The initial results demonstrate the synergy of the combined endoscopy over each modality alone.

OCT/laser-induced fluorescence

Laser-induced fluorescence (LIF) spectroscopy is a nondestructive imaging modality for studying molecular structures.[83] A laser is used to illuminate tissue and excite fluorophores such as structural proteins including collagen, metabolic co-factors nicotinamide adenine dinucleotide (NADH) and flavin adenine dinucleotide (FAD). LIF has shown diagnostic capabilities in ovarian cancer detection and characterization. Combined OCT/LIF has been used for imaging ovarian carcinogenesis rat models.[51,52] OCT images reveal normal and abnormal microstructural features and LIF provides biochemical information, which was able to characterize spectral differences in fluorescence emission attributed to collagen, NADH/FAD and hemoglobin absorption among cyclic ovaries, acyclic ovaries and sex cord-stromal tumors.

OCT/multiphoton microscopy

Multiphoton microscopy (MPM) is a nonlinear imaging technique based on light scanning to collect images of hundreds of microns in depth with submicron resolution.[84] The combined OCT/MPM system could provide information to evaluate structural changes by OCT, microscopic changes in fluorophore concentration by MPM two-photon excited fluorescence (TPEF), and collagen organization by MPM second harmonic generation (SHG). OCT/SHG in particular, is capable of imaging morphological features as well as collagen in ovarian tissue. The feasibility of *in vivo* imaging with OCT and MPM at multiple time points in a mouse model of ovarian tumorigenesis has been studied.[53] The researchers find evidence of microscopic changes over time associated with disease development in mouse ovarian tissue.

OCT/photoacoustic microscopy

Photoacoustic microscopy (PAM) is a photoacoustic imaging technique with micron-scale spatial resolution.[79,85] Optical-resolution PAM (OR-PAM) is capable of mapping microvasculature networks in biological tissue and resolving microvessels with much higher resolution than conventional photoacoustic images obtained with conventional ultrasound array transducers. The 3D PAM image can be obtained by performing 2D raster scan of the laser beam. Quantitative analysis of PAM ovarian tissue images achieved 88.2% sensitivity and 81.3% specificity for ovarian tissue diagnosis.[86] These preliminary results demonstrate the feasibility of PAM in mapping microvasculature networks for characterizing ovarian tissue. Combined 3D OCT/PAM imaging system has been implemented [87] and could be

accomplished by using a single broad-band laser source.[88] The potential of OCT combined with PAM for providing both scattering and absorption features of ovarian tissue will be investigated in the near future.

Discussion and Conclusion

The initial results of OCT and OCT in combination with other imaging modalities are promising. However, translating the *ex vivo* results to *in vivo* imaging has many challenges. First, OCT is limited to surface and subsurface examinations and can only be used before or during prophylactic oophorectomy procedures or as an exploratory surgery to determine if malignancy is present. Second, OCT scanning area is limited and full-field OCT (FF-OCT) is more desirable for quick diagnosis of ovarian tissue before making surgical decisions. In FF-OCT, the entire image filed is illuminated with a low spatial coherence light, it produces 2D *en-face* images using CCD or CMOS camera without scanning the light beam. FF-OCT is capable of imaging tissue at cellular level, and has been applied on imaging fresh and fixed tissues of breast tumors, sentinel nodes, skin, brain, kidney, lungs, and prostate.[89] However, FF-OCT has lower sensitivity and limited penetration depth. Although some fresh tissues can be imaged by FF-OCT, thin slices are always desirable for high image quality. Currently, we are investigating FF-OCT and other imaging modalities for quick scanning of a larger field of view before surgery. We envision that the major clinical application for OCT and OCT in combination with other imaging modalities is differentiating benign from malignant ovaries when a woman presents with an ovarian or pelvic mass. Frozen section is only 80% accurate and can only be done on an excised ovary. Transvaginal ultrasound has only a 1–3% positive predictive value for the diagnosis of an ovarian malignancy in low risk women and thus 97–99% of women with an abnormality on ultrasound do not have cancer at the time of surgery, thus conveying a false positive rate of 97–99%.[90] The ability, particularly in a young woman to preserve her ovary, would greatly benefit patients because there is increasing literature supporting the benefit of retaining a woman's ovaries until their mid 60's.[41,42,91–94] There is a significant survival benefit to avoiding oophorectomy and although the risk of ovarian cancer is reduced when both ovaries are removed all-cause mortality, fatal and nonfatal breast cancer, coronary heart disease, and lung cancer is significantly increased.

In summary, the use of OCT for ovarian tissue imaging and characterization is promising. OCT is capable of imaging microstructures of ovarian tissue, and providing imaging features that are different between normal, abnormal and malignant ovarian tissue. Quantitative analysis of OCT provides optical scattering properties and birefringence features of ovarian tissue, and demonstrates great potential for ovarian cancer diagnosis. The highly positive correlation between parameters extracted from OCT images and collagen content estimated from histology indicates that OCT is capable of measuring the complicated collagen development process in ovarian cancer. In addition, the combination of OCT with other imaging modalities provides additional information of ovarian tissue and has great potential of improving the accuracy of ovarian cancer diagnosis.

Acknowledgments

References

1. Fujimoto JG. Optical coherence tomography for ultrahigh resolution in vivo imaging. Nat Biotechnol. 2003; 21:1361–1367. [PubMed: 14595364]

2. Fercher AF, Drexler W, Hitzenberger CK, Lasser T. Optical coherence tomography-principles and applications. Rep Prog Phys. 2003; 66:239–303.

3. Tomlins PH, Wang RK. Theory, developments and applications of optical coherence tomography. J Phys D: Appl Phys. 2005; 38:2519–2535.

4. Drexler, W.; Fujimoto, JG. Optical coherence tomography: technology and applications. Springer; 2008.

5. Huang D, Swanson EA, Lin CP, Schuman JS, Stinson WG, Chang W, Hee MR, Flotte T, Gregory K, Puliafito CA, Fujimoto JG. Optical coherence tomography. Science. 1991; 254:1178–1181. [PubMed: 1957169]

6. Hee MR, Huang D, Swanson EA, Fujimoto JG. Polarization-sensitive low-coherence reflectometer for birefringence characterization and ranging. J Opt Soc Am B. 1992; 9:903–908.

7. de Boer JF, Milner TE. Review of polarization sensitive optical coherence tomography and Stokes vector determination. J Biomed Opt. 2002; 7:359–371. [PubMed: 12175285]

8. Chen Z, Zhao Y, Srinivas SM, Nelson JS, Prakash N, Frostig RD. Optical Doppler Tomography. IEEE J Sel Top Quantum Electron. 1999; 5:1134–1142.

9. Rollins AM, Yazdanfar S, Barton JK, Izatt JA. Real-time in vivo color Doppler optical coherence tomography. J Biomed Opt. 2002; 7:123–129. [PubMed: 11818020]

10. Piao D, Otis L, Zhu Q. Doppler angle and flow velocity mapping by combining Doppler shift and Doppler bandwidth measurements in optical Doppler tomography. Opt Lett. 2003; 28:1120–1123. [PubMed: 12879927]

11. Leitgeb R, Schmetterer L, Drexler W, Fercher A, Zawadzki R, Bajraszewski T. Real-time assessment of retinal blood flow with ultrafast acquisition by color Doppler Fourier domain optical coherence tomography. Opt Express. 2003; 11:3116–3121. [PubMed: 19471434]

12. Schmitt JM, Xiang SH, Yung KM. Differential absorption imaging with optical coherence tomography. J Opt Soc Am A. 1998; 15:2288–2296.

13. Morgner U, Drexler W, Kärtner FX, Li XD, Pitris C, Ippen EP, Fujimoto JG. Spectroscopic optical coherence tomography. Opt Lett. 2000; 25:111–113. [PubMed: 18059799]

14. Xu C, Carney P, Boppart S. Wavelength-dependent scattering in spectroscopic optical coherence tomography. Opt Express. 2005; 13:5450–5462. [PubMed: 19498540]

15. Fujimoto JG, Pitris C, Boppart SA, Brezinski ME. Optical coherence tomography: an emerging technology for biomedical imaging and optical biopsy. Neoplasia. 2000; 2:9–25. [PubMed: 10933065]

16. Vakoc BJ, Fukumura D, Jain RK, Bouma BE. Cancer imaging by optical coherence tomography: preclinical progress and clinical potential. Nat Rev Cancer. 2012; 12:363–368. [PubMed: 22475930]

17. Karanasos A, Ligthart J, Witberg K, van Soest G, Bruining N, Regar E. Optical coherence tomography: potential clinical applications. Curr Cardiovasc Imaging Rep. 2012; 5:206–220. [PubMed: 22798978]

18. Jaffe GJ, Caprioli J. Optical coherence tomography to detect and manage retinal disease and glaucoma. Am J Ophthalmol. 2004; 137:156–169. [PubMed: 14700659]

19. Yu L, Chen Z. Doppler variance imaging for three-dimensional retina and choroid angiography. J Biomed Opt. 2010; 15:016029. [PubMed: 20210473]

20. Li P, An L, Lan G, Johnstone M, Malchow D, Wang RK. Extended imaging depth to 12mm for 1050-nm spectral domain OCT for imaging whole anterior segment of human eye at 120 kHz A-scan rate. J Biomed Opt. 2013; 18:016012.

21. Otis LL, Everett MJ, Sathyam US, Colston BW Jr. Optical coherence tomography: a new imaging technology for dentistry. J Am Dent Assoc. 2000; 131:511–514. [PubMed: 10770016]

22. Holtzman JS, Osann K, Pharar J, Lee K, Ahn YC, Tucker T, Sabet S, Chen Z, Gukasyan R, Wilder-Smith P. Ability of optical coherence tomography to detect caries beneath commonly used dental sealants. Lasers Surg Med. 2010; 42:752–759. [PubMed: 20848554]

23. Chen YL, Yang Y, Ma J, Yan J, Shou Y, Wang T, Ramesh A, Zhao J, Zhu Q. 3D imaging of dental hard tissues with Fourier domain optical coherence tomography. Photonic Therapeutics and Diagnostics VII. Proc SPIE. 2011; 7883:78834O.

24. Testoni PA, Mangiavillano B. Optical coherence tomography in detection of dysplasia and cancer of the gastrointestinal tract and bilio-pancreatic ductal system. World J Gastroenterol. 2008; 14:6444–6452. [PubMed: 19030194]

25. Cobb MJ, Hwang JH, Upton MP, Chen YC, Oelschlager BK, Wood DE, Kimmey MB, Li X. Imaging of subsquamous Barrett's epithelium with ultrahigh-resolution optical coherence tomography: a histologic correlation study. Gastrointest Endosc. 2010; 71:223–230. [PubMed: 19846077]

26. Tearney GJ, Yabushita H, Houser SL, Aretz HT, Jang IK, Schlendorf KH, Kauffman CR, Shishkov M, Halpern EF, Bouma BE. Quantification of macrophage content in atherosclerotic plaques by optical coherence tomography. Circulation. 2003; 107:113–119. [PubMed: 12515752]

27. Barlis P, Serruys PW, Gonzalo N, van der Giessen WJ, de Jaegere PJ, Regar E. Assessment of culprit and remote coronary narrowings using optical coherence tomography with long-term outcomes. Am J Cardiol. 2008; 102:391–395. [PubMed: 18678293]

28. Bezerra HG, Costa MA, Guagliumi G, Rollins AM, Simon DI. Intracoronary optical coherence tomography: a comprehensive review clinical and research applications. JACC Cardiovasc Interv. 2009; 2:1035–1046. [PubMed: 19926041]

29. Shen B, Zuccaro G Jr, Gramlich TL, Gladkova N, Trolli P, Kareta M, Delaney CP, Connor JT, Lashner BA, Bevins CL, et al. In vivo colonoscopic optical coherence tomography for transmural inflammation in inflammatory bowel disease. Clin Gastroenterol Hepatol. 2004; 2:1080–1087. [PubMed: 15625653]

30. Boppart SA, Luo W, Marks DL, Singletary KW. Optical coherence tomography: feasibility for basic research and image-guided surgery of breast cancer. Breast Cancer Res Treat. 2004; 84:85–97. [PubMed: 14999139]

31. Mujat M, Ferguson RD, Hammer DX, Gittins C, Iftimia N. Automated algorithm for breast tissue differentiation in optical coherence tomography. J Biomed Opt. 2009; 14:034040. [PubMed: 19566332]

32. Curatolo A, McLaughlin RA, Quirk BC, Kirk RW, Bourke AG, Wood BA, Robbins PD, Saunders CM, Sampson DD. Ultrasound-guided optical coherence tomography needle probe for the assessment of breast cancer tumor margins. AJR Am J Roentgenol. 2012; 199:W520–522. [PubMed: 22997403]

33. Cancer Facts and Figures 2014. American Cancer Society; 2014.

34. Tammela J, Lele S. New modalities in detection of recurrent ovarian cancer. Curr Opin Obstet Gynecol. 2004; 16:5–9. [PubMed: 15128001]

35. Nossov V, Amneus M, Su F, Liang J, Janco JM, Reddy ST, Farias-Eisner R. The early detection of ovarian cancer: from traditional methods to proteomics. Can we really do better than serum CA-125. Am J Obstet Gynecol. 2008; 199:215–223. [PubMed: 18468571]

36. Van Calster B, Timmerman D, Bourne T, Testa AC, Van Holsbeke C, Domali E, Jurkovic D, Neven P, Van Huffel S, Valentin L. Discrimination between benign and malignant adnexal masses by specialist ultrasound examination versus serum CA-125. J Natl Cancer Inst. 2007; 99:1706–1714. [PubMed: 18000221]

37. Goozner M. Personalizing ovarian cancer screening. J Natl Cancer Inst. 2010; 102:1112–1113. [PubMed: 20668268]

38. Shaaban A, Rezvani M. Ovarian cancer: detection and radiologic staging. Clin Obstet Gynecol. 2009; 52:73–93. [PubMed: 19179862]

39. Kauff ND, Satagopan JM, Robson ME, Scheuer L, Hensley M, Hudis CA, Ellis NA, Boyd J, Borgen PI, Barakat RR, et al. Risk-reducing salpingo-oophorectomy in women with a BRCA1 or BRCA2 mutation. N Engl J Med. 2002; 346:1609–1615. [PubMed: 12023992]

40. Rebbeck TR, Lynch HT, Neuhausen SL, Narod SA, van't Veer L, Garber JE, Evans G, Isaacs C, Daly MB, Matloff E, et al. Prophylactic oophorectomy in carriers of BRCA1 or BRCA2 mutations. N Engl J Med. 2002; 346:1616–1622. [PubMed: 12023993]

41. Rocca WA, Grossardt BR, de Andrade M, Malkasian GD, Melton LJ. Survival patterns after oophorectomy in premenopausal women: a population-based cohort study. Lancet Oncol. 2006; 7:821–828. [PubMed: 17012044]

42. Berek JS, Chalas E, Edelson M, Moore DH, Burke WM, Cliby WA, Berchuck A. Prophylactic and risk-reducing bilateral salpingo-oophorectomy: recommendations based on risk of ovarian cancer. Obstet Gynecol. 2010; 116:733–743. [PubMed: 20733460]

43. Brewer MA, Utzinger U, Barton JK, Hoying JB, Kirkpatrick ND, Brands WR, Davis JR, Hunt K, Stevens SJ, Gmitro AF. Imaging of the ovary. Technol Cancer Res Treat. 2004; 3:617–627. [PubMed: 15560720]

44. Leitgeb R, Hitzenberger CK, Fercher AF. Performance of fourier domain vs. time domain optical coherence tomography. Opt Express. 2003; 11:889–894. [PubMed: 19461802]

45. Choma M, Sarunic M, Yang C, Izatt J. Sensitivity advantage of swept source and Fourier domain optical coherence tomography. Opt Express. 2003; 11:2183–2189. [PubMed: 19466106]

46. Yang Y, Biswal N, Wang T, Kumavor P, Karimeddini M, Vento J, Sanders M, Brewer M, Zhu Q. Potential role of a hybrid intraoperative probe based on OCT and positron detection for ovarian cancer detection and characterization. Biomed Opt Express. 2011; 2:1918–1930. [PubMed: 21750769]

47. Yang Y, Wang T, Biswal NC, Wang X, Sanders M, Brewer M, Zhu Q. Optical scattering coefficient estimated by optical coherence tomography correlates with collagen content in ovarian tissue. J Biomed Opt. 2011; 16:090504. [PubMed: 21950907]

48. Yang Y, Wang T, Brewer M, Zhu Q. Quantitative analysis of angle-resolved scattering properties of ovarian tissue using optical coherence tomography. J Biomed Opt. 2012; 17:090503.

49. Gamelin J, Yang Y, Biswal N, Chen Y, Yan S, Zhang X, Karemeddini M, Brewer M, Zhu Q. A prototype hybrid intraoperative probe for ovarian cancer detection. Opt Express. 2009; 17:7245–7258. [PubMed: 19399101]

50. Yang Y, Li X, Wang T, Kumavor P, Aguirre A, Shung K, Zhou Q, Sanders M, Brewer M, Zhu Q. Integrated optical coherence tomography, ultrasound and photoacoustic imaging for ovarian tissue characterization. Biomed Opt Express. 2011; 2:2551–2561. [PubMed: 21991547]

51. Kanter EM, Walker RM, Marion SL, Brewer M, Hoyer PB, Barton JK. Dual modality imaging of a novel rat model of ovarian carcinogenesis. J Biomed Opt. 2006; 11:041123. [PubMed: 16965151]

52. Hariri LP, Liebmann ER, Marion SL, Hoyer PB, Davis JR, Brewer MA, Barton JK. Simultaneous optical coherence tomography and laser induced fluorescence imaging in rat model of ovarian carcinogenesis. Cancer Biol Ther. 2010; 10:438–447. [PubMed: 21108515]

53. Watson JM, Marion SL, Rice PF, Bentley DL, Besselsen DG, Utzinger U, Hoyer PB, Barton JK. In vivo time-serial multi-modality optical imaging in a mouse model of ovarian tumorigenesis. Cancer Biol Ther. 2014; 15:42–60. [PubMed: 24145178]

54. Boppart SA, Goodman A, Libus J, Technician, Pitris C, Resear, Jesser CA, Brezinski ME, Fujimoto JG. High resolution imaging of endometriosis and ovarian carcinoma with optical coherence tomography: feasibility for laparoscopic-based imaging. Brit J Obstet Gynaec. 1999; 106:1071–1077.

55. Hariri LP, Bonnema GT, Schmidt K, Winkler AM, Korde V, Hatch KD, Davis JR, Brewer MA, Barton JK. Laparoscopic optical coherence tomography imaging of human ovarian cancer. Gynecol Oncol. 2009; 114:188–194. [PubMed: 19481241]

56. Evans CL, Rizvi I, Hasan T, de Boer JF. In vitro ovarian tumor growth and treatment response dynamics visualized with time-lapse OCT imaging. Opt Express. 2009; 17:8892–8906. [PubMed: 19466138]

57. Fine JL, Kagemann L, Wollstein G, Ishikawa H, Schuman JS. Direct scanning of pathology specimens using spectral domain optical coherence tomography: a pilot study. Ophthalmic Surg Lasers Imaging. 2010; 41:S58–S64. [PubMed: 21117602]

58. Korde VR, Liebmann E, Barton JK. Design of a handheld optical coherence microscopy endoscope. J Biomed Opt. 2011; 16:066018. [PubMed: 21721819]

59. Arifler D, Pavlova I, Gillenwater A, Richards-Kortum R. Light scattering from collagen fiber networks: micro-optical properties of normal and neoplastic stroma. Biophys J. 2007; 92:3260–3274. [PubMed: 17307834]

60. Faber D, van der Meer F, Aalders M, van Leeuwen T. Quantitative measurement of attenuation coefficients of weakly scattering media using optical coherence tomography. Opt Express. 2004; 12:4353–4365. [PubMed: 19483984]

61. Lee P, Gao W, Zhang X. Performance of single-scattering model versus multiple-scattering model in the determination of optical properties of biological tissue with optical coherence tomography. Appl Opt. 2010; 49:3538–3544. [PubMed: 20563206]

62. de Boer JF, Milner TE, van Gemert MJC, Nelson JS. Two-dimensional birefringence imaging in biological tissue by polarization-sensitive optical coherence tomography. Opt Lett. 1997; 22:934–936. [PubMed: 18185711]

63. Cense B, Chen TC, Park BH, Pierce MC, de Boer JF. Thickness and birefringence of healthy retinal nerve fiber layer tissue measured with polarization-sensitive optical coherence tomography. Invest Ophthalmol Vis Sci. 2004; 45:2606–2612. [PubMed: 15277483]

64. Elmaanaoui B, Wang B, Dwelle JC, McElroy AB, Liu SS, Rylander HG, Milner TE. Birefringence measurement of the retinal nerve fiber layer by swept source polarization sensitive optical coherence tomography. Opt Express. 2011; 19:10252–10268. [PubMed: 21643283]

65. Zotter S, Pircher M, Götzinger E, Torzicky T, Yoshida H, Hirose F, Holzer S, Kroisamer J, Vass C, Schmidt-Erfurth U, Hitzenberger CK. Measuring retinal nerve fiber layer birefringence, retardation, and thickness using wide-field, high-speed polarization sensitive spectral domain OCT. Invest Ophthalmol Vis Sci. 2013; 54:72–84. [PubMed: 23221076]

66. Fried D, Xie J, Shafi S, Featherstone JDB, Breunig TM, Le C. Imaging caries lesions and lesion progression with polarization sensitive optical coherence tomography. J Biomed Opt. 2002; 7:618–627. [PubMed: 12421130]

67. Chen Y, Otis L, Piao D, Zhu Q. Characterization of dentin, enamel, and carious lesions by a polarization-sensitive optical coherence tomography system. Appl Opt. 2005; 44:2041–2048. [PubMed: 15835353]

68. Nadkarni SK, Pierce MC, Park BH, de Boer JF, Whittaker P, Bouma BE, Bressner JE, Halpern E, Houser SL, Tearney GJ. Measurement of collagen and smooth muscle cell content in atherosclerotic plaques using polarization-sensitive optical coherence tomography. J Am Coll Cardiol. 2007; 49:1474–1481. [PubMed: 17397678]

69. Kuo W, Chou N, Chou C, Lai C, Huang H, Wang S, Shyu J. Polarization-sensitive optical coherence tomography for imaging human atherosclerosis. Appl Opt. 2007; 46:2520–2527. [PubMed: 17429466]

70. Strasswimmer J, Pierce MC, Park BH, Neel V, de Boer JF. Polarization-sensitive optical coherence tomography of invasive basal cell carcinoma. J Biomed Opt. 2004; 9:292–298. [PubMed: 15065894]

71. Sakai S, Yamanari M, Miyazawa A, Matsumoto M, Nakagawa N, Sugawara T, Kawabata K, Yatagai T, Yasuno Y. In vivo three-dimensional birefringence analysis shows collagen differences between young and old photo-aged human skin. J Invest Dermatol. 2008; 128:1641–1647. [PubMed: 18256690]

72. Sakai S, Yamanari M, Lim Y, Nakagawa N, Yasuno Y. In vivo evaluation of human skin anisotropy by polarization-sensitive optical coherence tomography. Biomed Opt Express. 2011; 2:2623–2631. [PubMed: 21991553]

73. Yang Y, Wang T, Wang X, Sanders M, Brewer M, Zhu Q. Quantitative analysis of estimated scattering coefficient and phase retardation for ovarian tissue characterization. Biomed Opt Express. 2012; 3:1548–1556. [PubMed: 22808427]

74. Wang T, Yang Y, Zhu Q. A three-parameter logistic model to characterize ovarian tissue using polarization-sensitive optical coherence tomography. Biomed Opt Express. 2013; 4:772–777. [PubMed: 23667792]

75. Piert M, Burian M, Meisetschläger G, Stein HJ, Ziegler S, Nährig J, Picchio M, Buck A, Siewert JR, Schwaiger M. Positron detection for the intraoperative localisation of cancer deposits. Eur J Nucl Med Mol Imaging. 2007; 34:1534–1544. [PubMed: 17431612]

76. Bogalhas F, Charon Y, Duval MA, Lefebvre F, Palfi S, Pinot L, Siebert R, Ménard L. Development of a positron probe for localization and excision of brain tumours during surgery. Phys Med Biol. 2009; 54:4439–4453. [PubMed: 19556688]

77. Piao D, Sadeghi MM, Zhang J, Chen Y, Sinusas AJ, Zhu Q. Hybrid positron detection and optical coherence tomography system: design, calibration, and experimental validation with rabbit atherosclerotic models. J Biomed Opt. 2005; 10:044010.

78. Xu M, Wang LV. Photoacoustic imaging in biomedicine. Rev Sci Instrum. 2006; 77:041101.

79. Wang LV, Hu S. Photoacoustic tomography: in vivo imaging from organelles to organs. Science. 2012; 335:1458–1462. [PubMed: 22442475]

80. Aguirre A, Ardeshirpour Y, Sanders MM, Brewer M, Zhu Q. Potential role of coregistered photoacoustic and ultrasound imaging in ovarian cancer detection and characterization. Transl Oncol. 2011; 4:29–37. [PubMed: 21286375]

81. Alqasemi U, Kumavor P, Aguirre A, Zhu Q. Recognition algorithm for assisting ovarian cancer diagnosis from coregistered ultrasound and photoacoustic images: ex vivo study. J Biomed Opt. 2012; 17:126003. [PubMed: 23208214]

82. Kumavor PD, Alqasemi U, Tavakoli B, Li H, Yang Y, Sun X, Warych E, Zhu Q. Co-registered pulse-echo/photoacoustic transvaginal probe for real time imaging of ovarian tissue. J Biophotonics. 2013; 6(6–7):475–484. [PubMed: 23450770]

83. Ramanujam N. Fluorescence spectroscopy of neoplastic and non-neoplastic tissues. Neoplasia. 2000; 2:89–117. [PubMed: 10933071]

84. Williams RM, Flesken-Nikitin A, Ellenson LH, Connolly DC, Hamilton TC, Nikitin AY, Zipfel WR. Strategies for high-resolution imaging of epithelial ovarian cancer by laparoscopic nonlinear microscopy. Transl Oncol. 2010; 3:181–194. [PubMed: 20563260]

85. Yao J, Wang LV. Photoacoustic microscopy. Laser Photon Rev. 2013; 7:758–778.

86. Wang T, Yang Y, Alqasemi U, Kumavor P, Wang X, Sanders M, Brewer M, Zhu Q. Characterization of ovarian tissue based on quantitative analysis of photoacoustic microscopy images. Biomed Opt Express. 2013; 4:2763–2768. [PubMed: 24409378]

87. Li L, Maslov K, Ku G, Wang LV. Three-dimensional combined photoacoustic and optical coherence microscopy for in vivo microcirculation studies. Opt Express. 2009; 17:16450–16455. [PubMed: 19770860]

88. Zhang X, Hao Zhang, Jiao S. Optical coherence photoacoustic microscopy: accomplishing optical coherence tomography and photoacoustic microscopy with a single light source. J Biomed Opt. 2012; 17:030502. [PubMed: 22502553]

89. Boccara C, Harms F, Latrive A. Full-field OCT: a non-invasive tool for diagnosis and tissue selection. SPIE Newsroom. 201310.1117/2.1201306.004933

90. Screening for ovarian cancer. Cancer Control. 2011; 18:16–21. [PubMed: 21273976]

91. Parker WH, Broder MS, Liu Z, Shoupe D, Farquhar C, Berek JS. Ovarian conservation at the time of hysterectomy for benign disease. Obstet Gynecol. 2005; 106:219–226. [PubMed: 16055568]

92. Parker WH, Broder MS, Liu Z, Shoupe D, Farquhar C, Berek JS. Ovarian conservation at the time of hysterectomy for benign disease. Clin Obstet Gynecol. 2007; 50:354–361. [PubMed: 17513923]

93. Shoupe D, Parker WH, Broder MS, Liu Z, Farquhar C, Berek JS. Elective oophorectomy for benign gynecological disorders. Menopause. 2007; 14:580–585. [PubMed: 17476148]

94. Parker WH, Broder MS, Chang E, Feskanich D, Farquhar C, Liu Z, Shoupe D, Berek JS, Hankinson S, Manson JE. Ovarian conservation at the time of hysterectomy and long-term health outcomes in the nurses' health study. Obstet Gynecol. 2009; 113:1027–1037. [PubMed: 19384117]
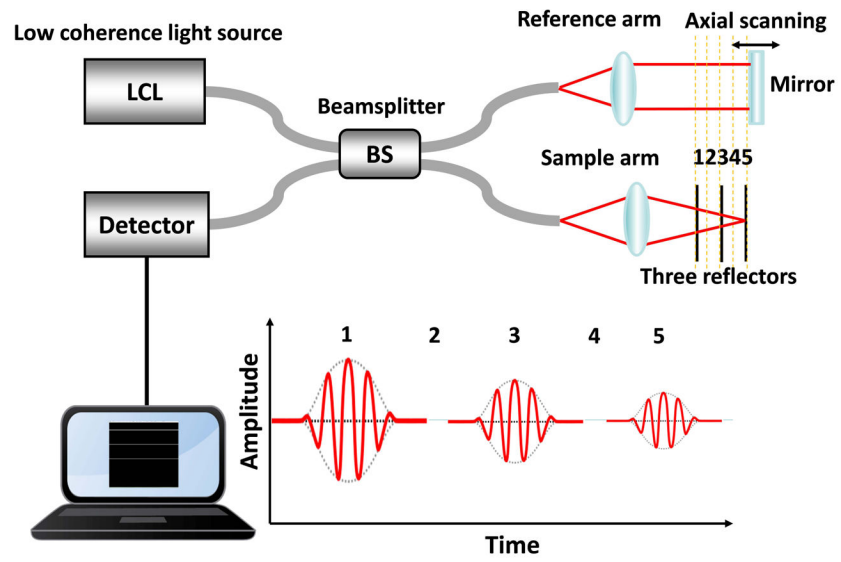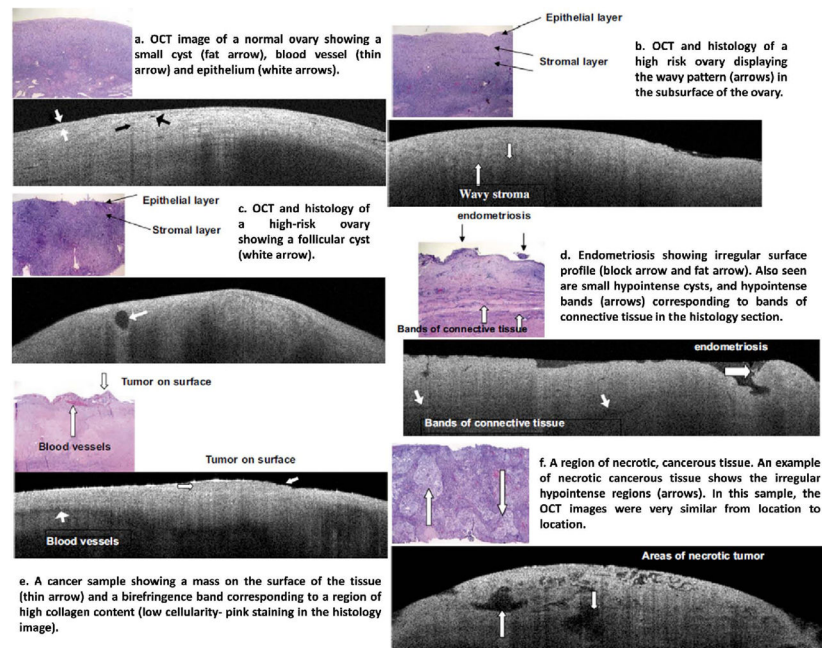
Figure 1.
OCT system configuration.

Figure 2.
OCT images and corresponding histology. The OCT images are 6 mm wide by 1.4 mm deep, the histology images are 2 mm wide by 1.5 mm deep. (Reprinted with permission from Ref 43. Imaging of the ovary, *Technol Cancer Res Treat* 3:617–627, 2004. Brewer MA, Utzinger U, Barton JK, Hoying JB, Kirkpatrick ND, Brands WR, Davis JR, Hunt K, Stevens SJ, Gmitro AF; http://www.tcrt.org)
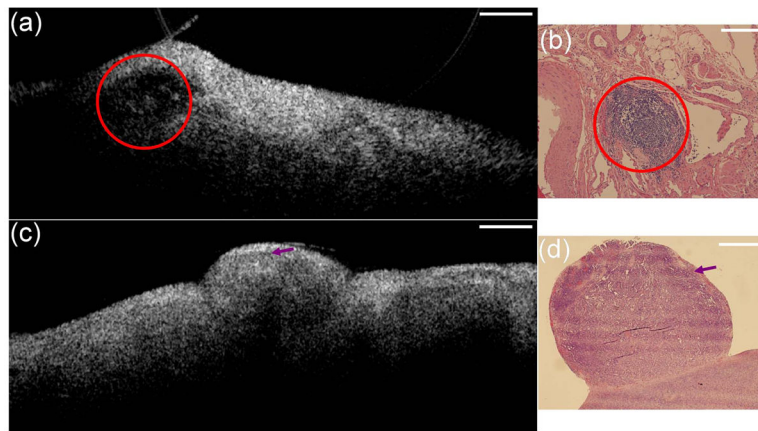
Figure 3.
(a) OCT image of ovary from an abnormal patient and (b) corresponding H&E histology; red circle: lymphocytes. (a) OCT image of ovary from patient with malignant ovarian cancers and (b) corresponding H&E histology; arrow: tumor nodule. Scale bar, 0.5 mm. (Reprinted with permission from Ref 46. Yang Y, Biswal N, Wang T, Kumavor P, Karimeddini M, Vento J, Sanders M, Brewer M, Zhu Q. Potential role of a hybrid intraoperative probe based on OCT and positron detection for ovarian cancer detection and characterization. *Biomed Opt Express* 2011, 2:1918–1930.)
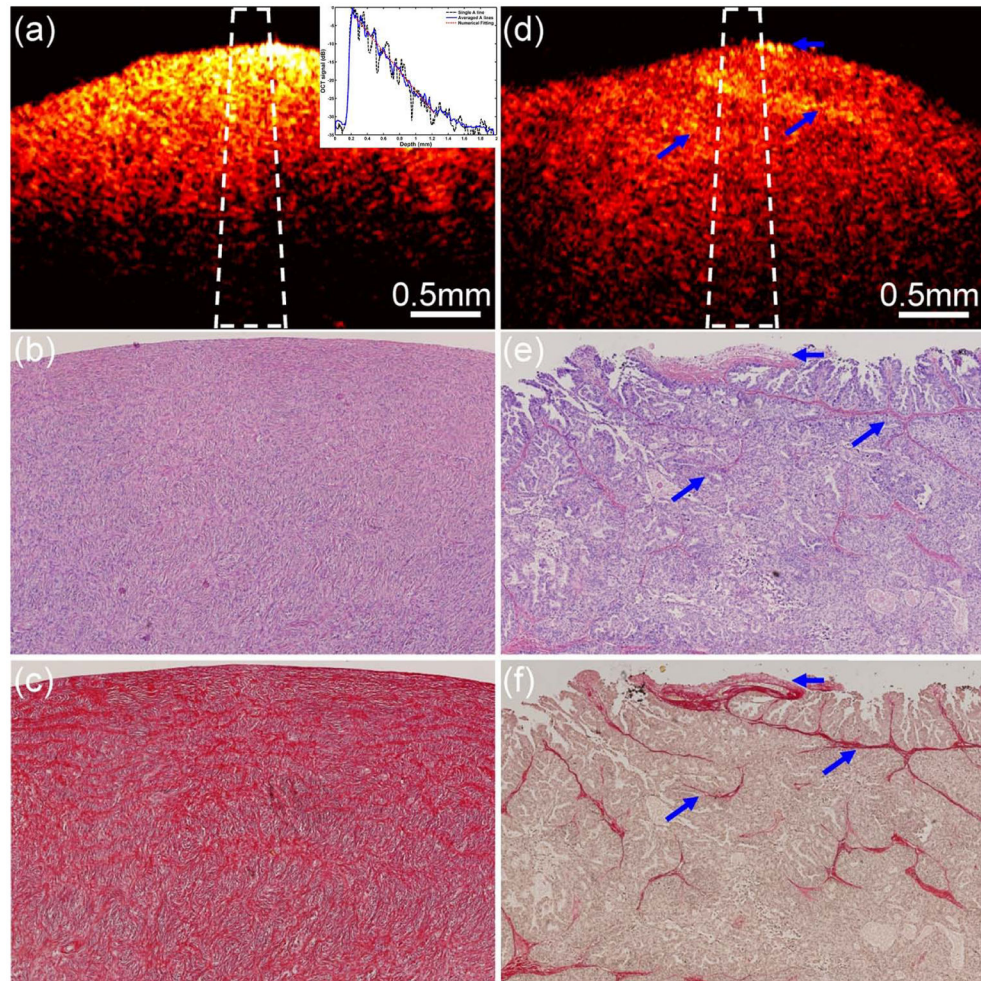
Figure 4.
One set of examples from normal (a–c) and malignant (d–f) ovarian tissue. (a), (d): OCT images; (b), (e): H&E histology; (c), (f): picrosirius red stains. Inset: fitting example; blue arrows: collagen bundles. (Reprinted with permission from Ref 47. Yang Y, Wang T, Biswal NC, Wang X, Sanders M, Brewer M, Zhu Q. Optical scattering coefficient estimated by optical coherence tomography correlates with collagen content in ovarian tissue. *J Biomed Opt* 2011, 16:090504.)
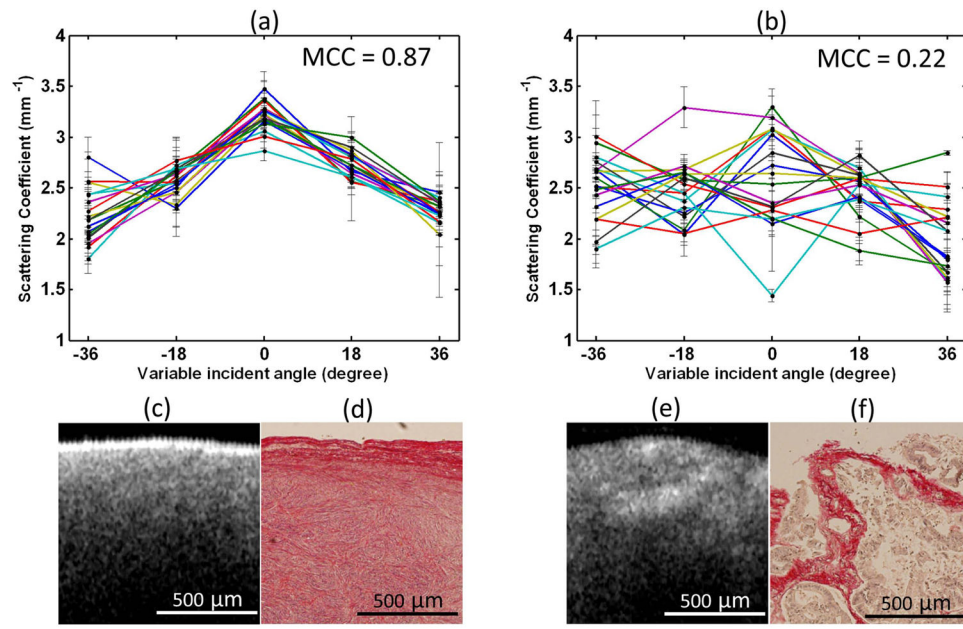
Figure 5.

Top: plots of angle-resolved scattering coefficients on 18 different OCT imaging planes from (a) normal ovarian tissue and (b) malignant ovarian tissue. Bottom: OCT images and picrosirius red histology images of normal ovarian tissue (c, d) and malignant ovarian tissue (e, f). (Reprinted with permission from Ref 48. Yang Y, Wang T, Brewer M, Zhu Q. Quantitative analysis of angle-resolved scattering properties of ovarian tissue using optical coherence tomography. *J Biomed Opt* 2012, 17:090503.)
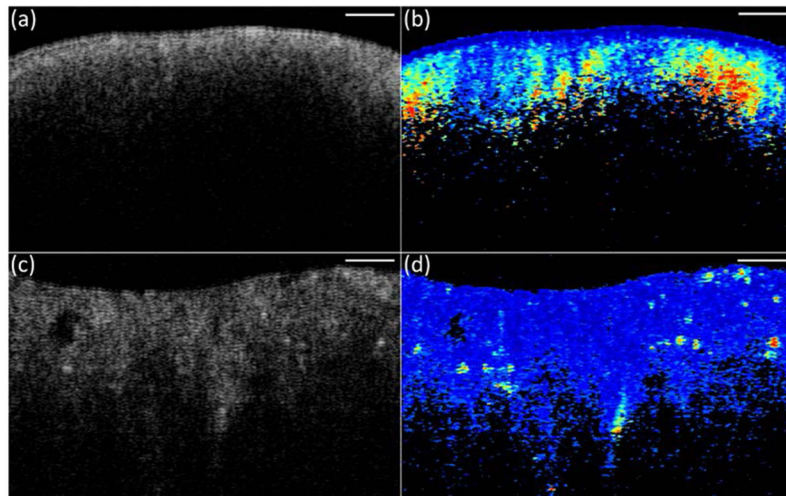
Figure 6.
Intensity OCT (a, c) and phase retardation images (b, d) from normal (a, b) and malignant (c, d) ovarian tissue. Scale bar, 0.5 mm. (Reprinted with permission from Ref 73. Yang Y, Wang T, Wang X, Sanders M, Brewer M, Zhu Q. Quantitative analysis of estimated scattering coefficient and phase retardation for ovarian tissue characterization. *Biomed Opt Express* 2012, 3:1548–1556.)
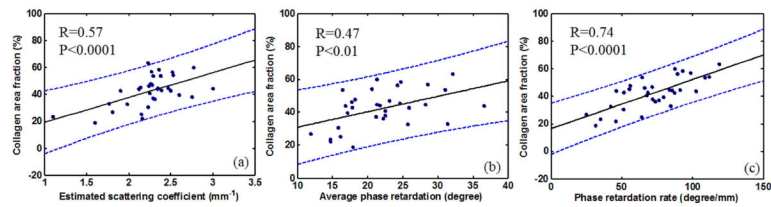
Figure 7.
Demonstration of positive correlation between (a) scattering coefficient, (b) phase retardation, (c) phase retardation rate, and collagen content; the blue dashed lines show 95% confidence intervals. (Reprinted with permission from Ref 73, Yang Y, Wang T, Wang X, Sanders M, Brewer M, Zhu Q. Quantitative analysis of estimated scattering coefficient and phase retardation for ovarian tissue characterization. *Biomed Opt Express* 2012, 3:1548–1556; and Ref 74 Wang T, Yang Y, Zhu Q. A three-parameter logistic model to characterize ovarian tissue using polarization-sensitive optical coherence tomography. *Biomed Opt Express* 2013, 4:772–777.)
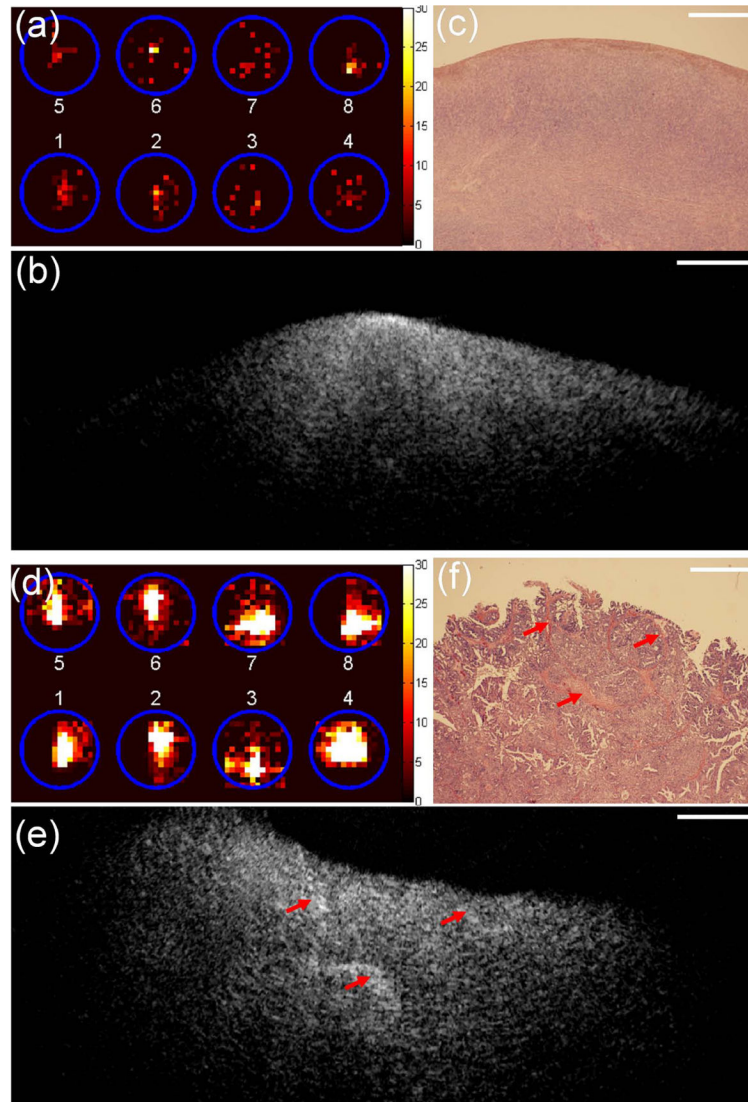
Figure 8.
(a)–(c), one set of images obtained from one ovary of normal patient. (d)–(f) One set of
images obtained from one ovary of patient with ovarian cancers. (a, d) Positron distribution
map; (b, e) OCT image; (c, f) corresponding H&E histology; scale bar, 0.5 mm. (Reprinted
with permission from Ref 46. Yang Y, Biswal N, Wang T, Kumavor P, Karimeddini M,
Vento J, Sanders M, Brewer M, Zhu Q. Potential role of a hybrid intraoperative probe based
on OCT and positron detection for ovarian cancer detection and characterization. *Biomed
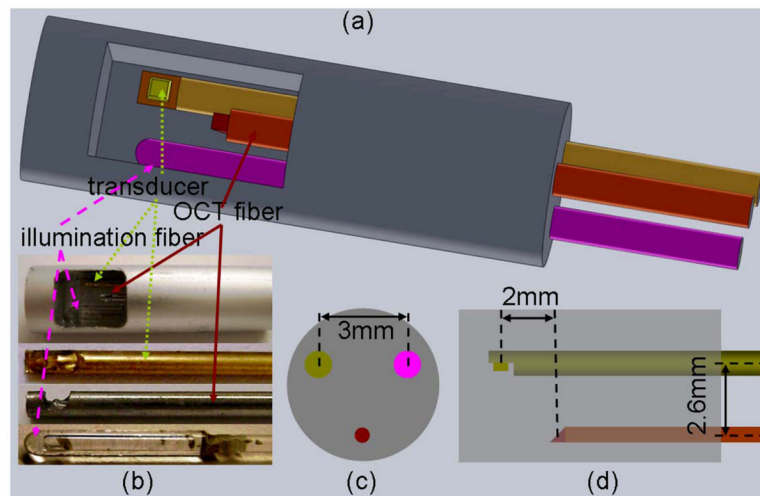Opt Express* 2011, 2:1918–1930.)

Figure 9.
Integrated OCT-US-PAI three-modality endoscopic probe. (a) Sketch of the three-modality probe; (b) photographs of probe and components (transducer, OCT fiber and light illumination fiber); (c) left view of the probe configuration; (d) side view of the probe configuration. (Reprinted with permission from Ref 50. Yang Y, Li X, Wang T, Kumavor P, Aguirre A, Shung K, Zhou Q, Sanders M, Brewer M, Zhu Q. Integrated optical coherence tomography, ultrasound and photoacoustic imaging for ovarian tissue characterization. *Biomed Opt Express* 2011, 2:2551–2561.)
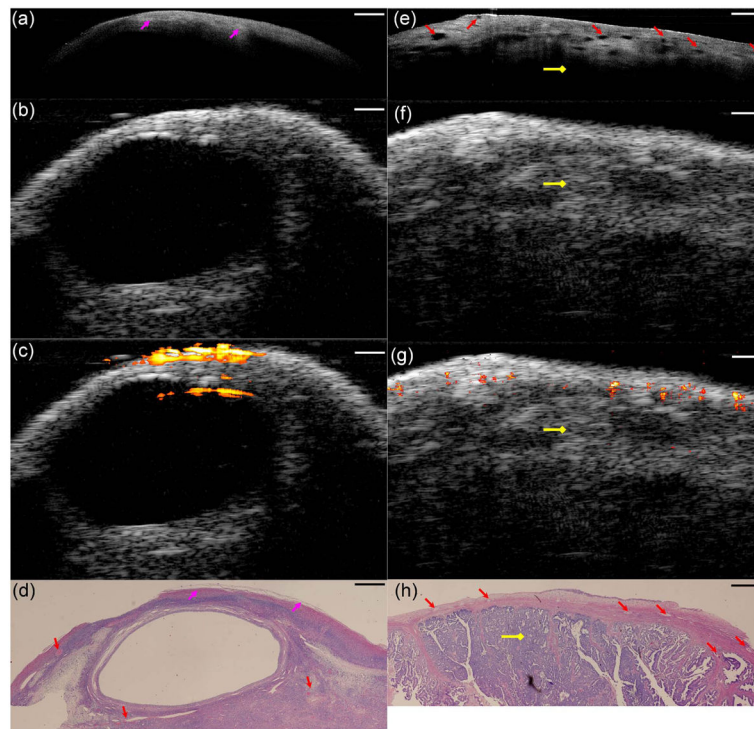
Figure 10.
(a)–(d) One set of images of ovarian tissue from a patient with endometriosis. (e)–(h) One set of images of malignant ovarian tissue from a 61-year old patient. (a, e) OCT image; (b, f) US image; (c, g) superimposed PAI and US image; (d, h) corresponding histology. Pink arrow, collagen bundle; red stealth arrow, blood vessel; yellow diamond arrow, malignant tissue; scale bar, 1mm. (Reprinted with permission from Ref 50. Yang Y, Li X, Wang T, Kumavor P, Aguirre A, Shung K, Zhou Q, Sanders M, Brewer M, Zhu Q. Integrated optical coherence tomography, ultrasound and photoacoustic imaging for ovarian tissue characterization. *Biomed Opt Express* 2011, 2:2551–2561.)